# Observation of Absorption-Dominated Bonding Dark Plasmon Mode from Metal–Insulator–Metal Nanodisk Arrays Fabricated by Nanospherical-Lens Lithography

**Yun-Chorng Chang,* Shih-Ming Wang, Hsin-Chan Chung, Chung-Bin Tseng, and Shih-Hui Chang**

Department of Photonics and Advanced Optoelectronic Technology Center, National Cheng Kung University, Tainan 701, Taiwan

**ABSTRACT**

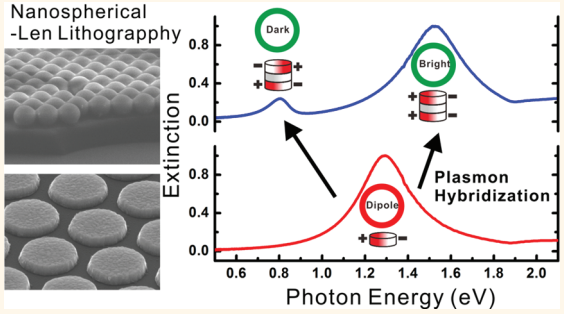


**Plasmon hybridization modes are observed in the extinction spectra of a metal–insulator–metal (MIM) nanodisk array fabricated using nanospherical-lens lithography. Two distinct hybridization modes are observed in this vertically aligned configuration. Theoretical simulation indicates that the bonding mode located at a lower energy level exhibits an antiphase charge distribution and corresponds to the dark plasmon mode. This is vastly different compared to antibonding dark plasmon mode observed in the conventional dimer configuration. The observed mode is tunable over a wide spectral range simply by varying the insulator thickness and the diameters of the MIM nanodisks. Absorption is the dominating extinction process for the dark plasmon, while scattering dominates the bright plasmon mode. The ability to experimentally measure and tune dark plasmon modes using a MIM configuration should catalyze more novel studies that take full advantages of the absorption-dominated dark plasmon mode.**

**KEYWORDS:** nanodisk · MIM · nanosphere · surface plasmon · dark plasmon

Surface plasmons (SPs) are collective oscillations of conductive electrons propagating at the metal surface.[1,2] Surface plasmons in a noble metal nanoparticle are highly localized at the surface of the nanoparticle and decay rapidly away from the surface, which is referred to as localized surface plasmon resonances (LSPR). The far-field light scattering induced by LSPR is very sensitive to the dielectric environment and is widely used in ultrasensitive chemical and biological sensing applications.[3–6]

LSPR of an individual nanoparticle can be tuned by varying the size and shape of the nanoparticle.[7] The strong electric field enhancement at the surface is ideal for surface-enhanced Raman scattering (SERS).[8] Recently, plasmonic dimers have become an important topic due to the tunable surface plasmon resonance (SPR) when changing the interparticle distance. The plasmonic coupling between metal nanoparticles exhibits strong electric field enhancement between the nanoparticle pairs and has the potential to significantly improve the sensitivity of SERS.[9] The plasmonic coupling is explained by the plasmon hybridization model introduced by Prof. Nordlander and co-workers.[10–12] The coupling between nanoparticle pairs is considered as the coupling between the LSPR of individual nanoparticles, which is analogous to the bonding and antibonding splitting in molecular orbital theory. The bonding mode in a dimer configuration, located at a lower energy level, interacts strongly with the incident radiation and is thus referred to as the "bright" plasmon mode. The antibonding mode, located at a higher energy level, has zero net dipole moment and is referred to as the "dark" plasmon mode. The optically active bright plasmon mode strongly scatters incident light and has already been extensively researched and used in many applications. The bright plasmon mode can rapidly deplete the plasmon energy, which prevents further enhancement of local optical fields.[13] The dark

* Address correspondence to ychang6@mail.ncku.edu.tw.

Received for review January 29, 2012 and accepted March 21, 2012.

**Published online March 21, 2012**
**10.1021/nn300420x**

plasmon mode, which exhibits a longer lifetime, is better suited for applications such as plasmonic nanolaser applications.[14,15] However, the dark plasmon observed so far cannot be tuned over a broad wavelength region, which limits the development of dark-plasmon-related applications.

A conventional plasmonic dimer consists of a pair of nanoparticles that are sitting side-by-side on top of a substrate and separated by a very short distance (<100 nm). To measure the optical extinction spectra for this plasmonic dimer, the incident light is introduced at an incident angle normal to the substrate surface. In such a case, the incident electric field of light resides in the plane of supporting substrate and the antibonding dark plasmon mode cannot be excited through this configuration. Therefore, only the bonding bright plasmon mode can be observed. Figure 1a and b schematically illustrate this concept. The difficulty in exciting the dark plasmon mode has severely limited our understanding of the nature of the dark plasmon mode, and only a few researchers have been able to experimentally observe the dark plasmon mode by using polarization-selective total internal reflection spectroscopy[16] or electron energy-loss spectroscopy.[17−19] Recently, it was proposed that the dark plasmon mode of a gold nanoring can be observed when incident light illuminates at an oblique angle. The retardation effect of light due to the large nanoring is considered to be crucial for the excitation of the dark plasmon mode.[20]

Metal−insulator−metal (MIM) nanodisks consist of metal nanodisks that are aligned vertically and separated by a thin insulating dielectric layer. MIM nanodisks have been studied considerably in several nanophotonic fields. For example, MIM nanodisks were recognized as nanoplasmonic resonator sensors for SERS, whose plasmon resonance can be tuned by changing the insulator thickness.[21,22] MIM nanodisks were also studied as magnetic metamaterials and demonstrated negative $\mu$ at a wavelength of 1.2 $\mu$m.[23] A high Purcell factor was observed due to the ultrasmall mode volume in a MIM nanodisk, which should be very important for applications such as nanolasers.[24] Despite all these research efforts, MIM nanodisks recognized as a vertically aligned plasmonic dimer were rarely reported. A commercial spectrophotometer was used in this study to observe the dark plasmon mode of MIM nanodisk arrays, whose resonance is in the near-infrared region. Expensive nanofabrication methods, such as focused-ion-beam milling or electron-beam lithography, are not practical methods to fabricate the necessary large (>1 mm$^2$) sampling area. Fabrications of nanodisk arrays that cover a large area were reported using interference lithography[23] and nanoimprint lithography.[25] Nanosphere lithography has also been developed to fabricate nanoscale triangle prisms.[26] The application of a nanosphere as a phase-shifting lithography mask to fabricate two-dimensional[27,28] or three-dimensional[29] nanostructures was previous reported. This method uses nanospheres as a nanoscale spherical lens to focus the incident UV light to obtain nanoscale exposure photoresist patterns, which is referred to as nanospherical-lens lithography (NLL).

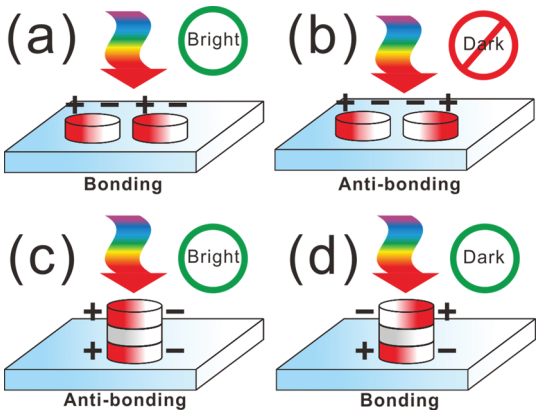


**Figure 1. Schematic illustrations of the mode excitation for (a, b) a horizontally aligned nanoparticle dimer and (c, d) a vertically aligned metal−insulator−metal (MIM) nanodisk. The vertically incident light cannot excite the dark plasmon mode for a nanoparticle dimer in (b). The same incident light is able to excite the dark plasmon in a MIM nanodisk in (d) due to the addition phase delay introduced by the insulator layer.**

In this research, large-area Ag nanodisks and MIM nanodisk arrays are successfully fabricated using nanospherical-lens lithography. The absorption spectra for MIM nanodisk arrays reveal both the antibonding and bonding modes predicted by plasmon hybridization theory. It is surprising to find out that the bonding mode reveals an antiphase charge distribution and corresponds to the dark plasmon mode. This is vastly different compared with the antibonding dark plasmon mode in a conventional dimer configuration. Tuning of the dark plasmon mode can be easily achieved by varying the insulator thickness and the nanodisk diameters. In addition, we also report that absorption is the dominant process for this dark plasmon mode, and the bright plasmon mode is dominated by scattering. Results in this study should catalyze more research results that take advantage of this absorption-dominated dark plasmon mode in a MIM nanodisk configuration.

## RESULTS AND DISCUSSION

**Metal−Insulator−Metal Nanodisk Arrays Fabricated Using Nanospherical-Lens Lithography.** Nanospheres with diameters of 500 nm function as nanoscale lenses to focus incident UV light. This nanosphere array acts as a lithography mask that collimates the uniformly illuminated UV exposure light into a cylindrical light pattern, which results in perfectly round nanodisks after subsequent metal deposition and lift-off processes.

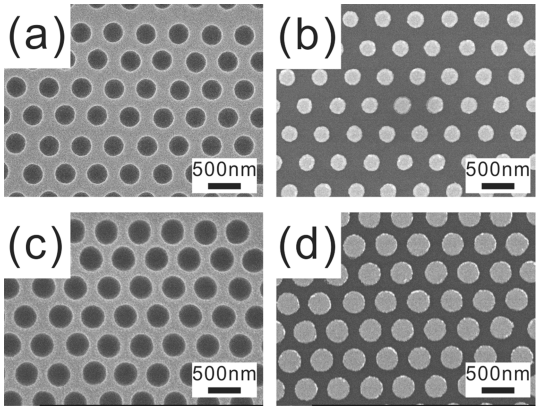


**Figure 2. SEM images of the photoresist patterns of the (a) as-developed and (c) after 50 s oxygen plasma treatment. (b and d) Corresponding metal nanodisk arrays after 25 nm Ag deposition and metal lift-off.**

Detailed fabrication procedures are described in the Methods section. The diameter of the nanodisk can be tuned by controlling the exposure and developing time of the photoresist (PR) in NLL. In addition, oxygen plasma is also used to alter the diameter of the nanodisk, as illustrated in the scanning electron microscopy (SEM) images shown in Figure 2. The diameters of the PR holes and nanodisks after 50 s of oxygen plasma treatment, shown in Figure 2c and d, are larger than the untreated cases shown in Figure 2a and b. These SEM images demonstrate that NLL can economically fabricate high-quality nanodisks that cover large areas.

**Plasmon Hybridization Observed in the Transmission Spectra of MIM Nanodisk Arrays.** MIM nanodisks that consist of a Ag film (thickness = 15 nm) and a $SiO_2$ film of various thicknesses (10, 15, and 20 nm) were also fabricated using NLL. The periodicity is 500 nm, and the diameter of the fabricated nanodisks is 260 nm. The simulated and experimental extinction spectra of these arrays are illustrated in Figure 3a and b, respectively. In both figures, the surface plasmon resonance for single-layer Ag nanodisk arrays is located around 1.3 eV. In the spectra of MIM nanodisks, an additional extinction band appears around 0.6 eV. When the thickness of $SiO_2$ increases, the peak position of this band shifts to higher energy, which results in a smaller energy difference between these two peaks. According to the plasmon hybridization theory, the energy splitting becomes smaller when the interparticle distance increases due to the reduced coupling strength. Therefore, this additional blue-shifting peak should correspond to the bonding plasmon mode. The wavelength of the antibonding mode is around ~750 nm, which is very close to the periodicity of the nanodisk arrays (period = 500 nm, $n_{substrate}$ = 1.5). The periodic effect has caused the red-shifting of the antibonding plasmon mode not to be very distinct. In addition, the resonance peaks in the experimental results all exhibit

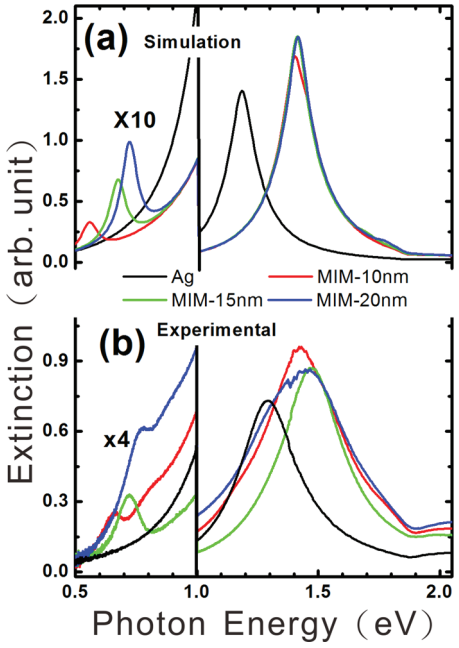


**Figure 3. (a) Simulated and (b) experimental extinction spectra for Ag and Ag−$SiO_2$−Ag MIM nanodisk ($T_{ag}$ = 15 nm, $T_{SiO2}$ = 10, 15, 20 nm) with diameters of ~260 nm. Plasmon hybridization is observed in both figures. The low-energy sides of both spectra are intentionally enlarged to demonstrate the shift of the dark plasmon mode when varying the insulator thickness.**

a broader line width compared to the simulated results, which is due to particle size inhomogeneities. However, this should not be a problem in this study since the peak locations and the shifts of these modes are clearly observable in the experimental results.

**Bonding Mode Corresponds to Dark Plasmon Mode.** In Figure 3, we have noticed that the bonding mode located at a lower energy level exhibits a narrower line width, which usually corresponds to the dark plasmon mode. However, the bonding mode in a conventional dimer configuration corresponds to the bright plasmon mode. In order to determine the accurate plasmon hybridization modes, the charge distributions of the MIM nanodisk are simulated when illuminated with light of photon energy of 1.5 and 0.75 eV, shown in Figure 4a and b, respectively. In Figure 4a, the charge distribution of the top and bottom Ag nanodisks reveals an in-phase configuration when illuminated with 1.5 eV photons, which corresponds to the bright plasmon mode. By contrast, the charge distribution of the top and bottom Ag nanodisks reveals an antiphase configuration when illuminated with 0.75 eV photons, shown in Figure 4b. This antiphase charge distribution indicates that the extinction peak located at 0.75 eV corresponds to the dark plasmon mode, which is surprising since the dark plasmon mode in a horizontally aligned dimer configuration corresponds to the antibonding mode. This result serves as a rare example where the dark plasmon mode does not have to be an

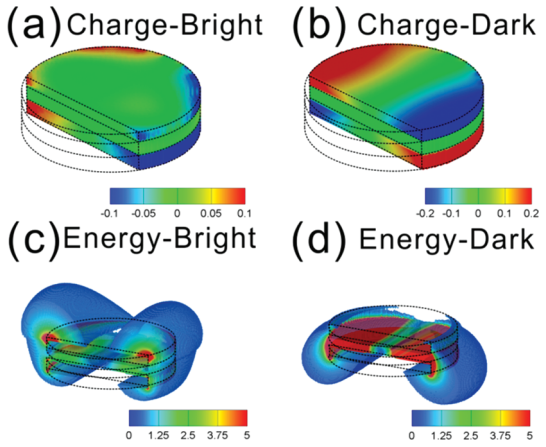


Figure 4. Simulated charge distributions of the MIM nanodisk when illuminating with light of photon energy of (a) 1.5 eV and (b) 0.75 eV. The corresponding simulated field energy distributions are shown in (c) and (d), respectively. Part of the distribution pattern in each figure is intentionally removed to illustrate the distribution inside the MIM nanodisk. The black, dashed lines indicate the outline of the nanodisk. The top surface attaches to the glass substrate.

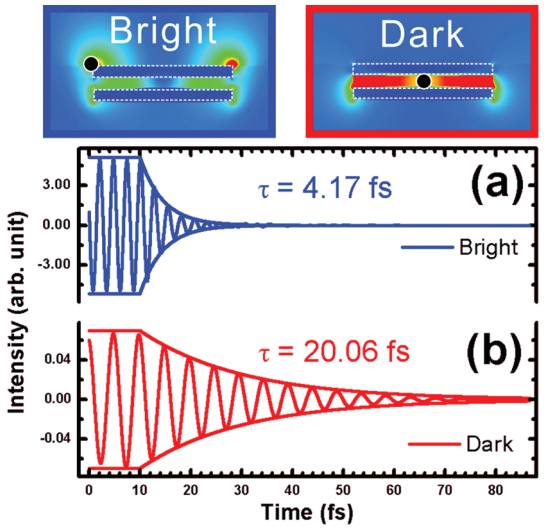


Figure 5. Temporal evolutions of the simulated electric field intensity for the (a) bright and (b) dark plasmon modes of a Ag−$SiO_2$−Ag nanodisk ($D$ = 240 nm) after the light source is turned off. Thickness of all three layers is 10 nm. The black dot indicates the detection point for each case. The decay time is longer for the dark plasmon mode.

antibonding mode. It can be either an antibonding or bonding mode depending on the dimer configuration.

**Dark Plasmon Mode Exhibits a Longer Electric Lifetime.** The narrower dark plasmon mode should exhibit a much longer decay time compared with the bright plasmon mode. The temporal evolutions of the electric field are simulated for both modes, and the results are shown in Figure 5. Ag−$SiO_2$−Ag nanodisks are used in this simulation, and the thickness for each layer is 10 nm. The periodicity is 500 nm, and the disk diameter is 240 nm. In both simulations, the light source is turned off when the electric field at the detection point, whose

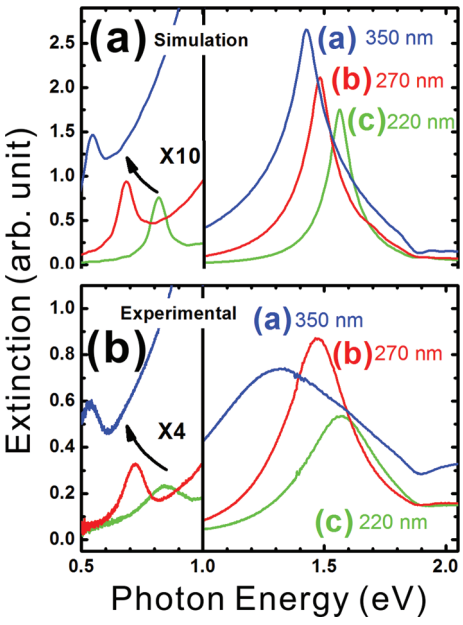


Figure 6. (a) Simulated and (b) experimental extinction spectra of MIM nanodisk arrays with different diameters. The periodicity is set at 500 nm.

location is indicated as a black dot in Figure 5, reaches steady state. The bright plasmon mode decays very quickly after the light source is turned off, as shown in Figure 5a. The decay time constant is estimated to be 4.17 fs. The decay of the dark plasmon mode is also monitored, which is shown in Figure 5b. The decay is not as fast for the dark plasmon mode, and the decay time is estimated to be 20 fs, which is 5 times longer than the bright plasmon mode. The simulation results confirm that the dark plasmon mode exhibits a longer electric field lifetime and should be beneficial for applications such as plasmon-enhanced florescence and nanoscale lasing.

**Tuning the Dark Plasmon Mode by Varying the Nanodisk Diameters and Interdisk Gap Distance.** Another important advantage of the MIM configuration is the ability to tune the resonance frequency of the dark plasmon mode. It has been demonstrated in Figure 3 that changing the insulator thickness varies the resonance frequency. Fine tuning is possible because we can deposit a very precise thickness using current thin-film deposition technologies. In addition, we also found that the dark plasmon mode can be tuned by changing the diameter of the nanodisk arrays. The simulated and experimental extinction spectra are shown in Figure 6. The dark plasmon mode shifts from 0.85 to 0.55 eV when the diameter of the nanodisk increases from 220 to 350 nm. Fine tuning of the nanodisk diameter and the resonance frequency can be further achieved by oxygen plasma treatment, which has been illustrated in Figure 2. The precise and wide tuning range of the dark plasmon mode by controlling the diameters of the nanodisk should be very important since we can easily

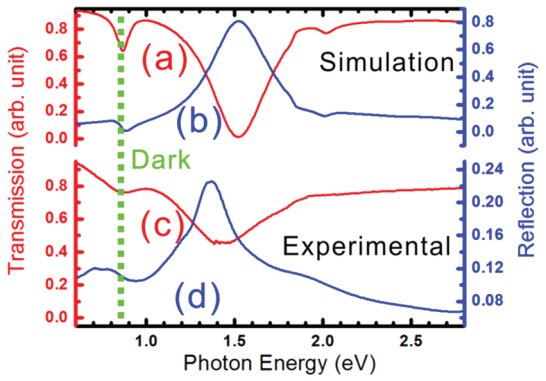


**Figure 7. Simulated transmission (a), reflection (b), experimental transmission (c), and absorption (d) spectra of Ag (15 nm)−$SiO_2$(25 nm)−Ag (15 nm) nanodisk ($D$ = 240 nm) arrays. The periodicity is 500 nm. Reflection is very little at the dark mode resonance near 0.75 eV.**

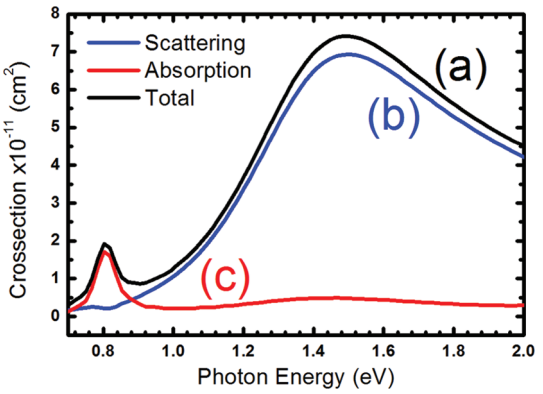


**Figure 8. Simulated extinction spectra for a Ag−$SiO_2$−Ag MIM nanodisk ($T_{ag}$ = 15 nm, $T_{SiO2}$ = 15 nm). (a) Total extinction spectrum, which is the sum of the scattering spectrum (curve b) and the absorption spectrum (curve c).**

tune the dark plasmon mode to match a specific application or excitation frequency.

**Dark Plasmon Mode Cannot Be Observed through a Dark-Field Configuration.** The MIM nanodisk is a common configuration that has been studied for several other applications. It has surprised us to find out that no one has reported the observation of the dark plasmon mode using the MIM configuration. We believe this is due to two factors. First, the dipole mode for a Ag nanodisk with a diameter of 200 nm is located near 1.55 eV. According to the hybridization theory, the bonding mode will shift to a lower energy level and easily exceed the detection limit for a silicon-based photodetector, preventing the bonding mode from being observed in a conventional dark-field microscope. Extinction spectra for such a spectral range are usually measured by a commercial visible-NIR spectrophotometer, which requires a large (>1 mm$^2$) sampling area. It is not very practical to fabricate such arrays using focused-ion-beam milling or electron-beam lithography. In order to observe this phenomenon, fabrication of nanodisk arrays that cover a large area is essential, which limits the possibility for the dark plasmon mode to be observed and reported. Second, a dark-field microscope detects the backscattering light from the nanodisks. We believe that the dark plasmon mode does not scattering light and thus is not visible in a dark-field microscope. This point of view is further verified in the simulated and experimental reflection spectra of the MIM nanodisk arrays shown in Figure 7. Curves a and c in Figure 7 are the simulated and experimental transmission spectra of a Ag(15 nm)−$SiO_2$(25 nm)−Ag(15 nm) nanodisk array. The periodicity and the diameter of the nanodisk are 500 and 240 nm, respectively. The dark plasmon resonance mode is observable at 0.75 eV in both transmission spectra. However, very little reflection is observed at 0.75 eV in both the simulated (curve a) and experimental reflection spectra (curve d). The reflection spectra indicate that the dark plasmon mode of the MIM nanodisk arrays is not detectable under a dark-field microscope. Optical absorption spectroscopy is one of the very few methods able to detect this dark plasmon mode.

**Absorption-Dominated Dark Plasmon Mode and Scattering-Dominated Bright Plasmon Mode.** Figure 4c and d are the simulated field energy distributions when illuminating with light of photon energies of 1.5 and 0.75 eV, respectively. In Figure 4c, most of the field energy is distributed outside of the MIM nanodisk, which corresponds to the strong optical scattering by the bright plasmon mode. The field energy distribution of the dark plasmon mode, shown in Figure 4d, is strongly confined within the region between the Ag nanodisks. This also confirms that the dark plasmon mode will not strongly scatter the incident light and light absorption should be the dominating process. Therefore, the simulated scattering and absorption spectra of a single MIM nanodisk are obtained and shown in Figure 8. The diameter of the MIM nanodisk is 270 nm, and the thickness for each layer is 15 nm. The total extinction spectrum, shown as curve a, exhibits two separate peaks located near 1.5 and 0.8 eV. The scattering spectrum, shown as curve b, is dominated by the response from the bright plasmon mode located near 1.5 eV. Curve c corresponds to the absorption spectrum, which is dominated by the response from the dark plasmon mode located near 0.8 eV. The simulated spectra again verify our prediction that the dark plasmon mode will not strongly scatter the incident light, and it will be difficult to detect using dark-field microscopy. These results also indicate that the absorption and scattering process can be effectively separated using the MIM configuration, which should be beneficial for applications that use either the absorption or scattering process. In these applications, the other process usually serves as a problem that needs to be reduced. The MIM configuration is perfect to solve this dilemma.

## CONCLUSION

Plasmonic hybridization is observed from the absorption spectra of the MIM nanodisk arrays fabricated using nanospherical-lens lithography. The vertically incident light cannot excite the antibonding plasmon mode from a conventional dimer configuration, but it can excite both plasmon modes using the proposed MIM configuration. These concepts are schematically illustrated in Figure 1. The two observed plasmon modes are later identified as the antibonding bright and bonding dark plasmon modes, which is different from the antibonding dark plasmon mode that exists in a conventional dimer configuration. The dark plasmon mode is precisely tunable over a wide spectral region simply by changing the interdisk thickness or the diameters of the nanodisk. The ability to measure and tune the dark plasmon mode by using a MIM configuration should be beneficial for future applications that require a specific excitation wavelength. In addition, we also found that the dark plasmon mode is dominated by absorption, while the bright plasmon mode is dominated by scattering. The separation of the absorption- and scattering-dominated processes should also be useful for some specific applications. This dark plasmon mode also reflects very little light, which is why it was not previously observed by a dark-field microscope. Overall, we believe the MIM nanodisk configuration should help us to understand more about the dark plasmon mode and also catalyze more research results that take full advantage of the absorption-dominated dark plasmon mode.

## METHODS

**Sample Fabrication.** Quartz or silicon substrates that were cut into a size of $10 \times 10$ mm$^2$ were used in this study. After being ultrasonically cleaned in isopropyl alcohol, the substrates were rinsed with deionized water and subsequently blow-dried by nitrogen. The nanospheres used in this study were polystyrene spheres with diameters of 500 and 1000 nm (Polyscience Inc.). First, a thin layer of photoresist was spin-coated on top of the substrate followed by soft-baking at 90 °C for 3 min. The estimated thickness of the PR was about 1 $\mu$m. Nanospheres were self-assembled into a single-layered hexagonal close-packed array by using a convective self-assembly method.[30] After the formation of nanosphere masks, the samples were exposed to ultraviolet (UV) light ($\lambda$ = 365 nm) using a commercial mask aligner (Karl Suss, MJB4). Following the exposure process, the exposed-PR thin film was developed and the remaining nanospheres were removed. Ag or Ag−$SiO_2$−Ag thin films were thermally evaporated or sputtered onto the samples. Nanodisk arrays were revealed after the lift-off process.

**Experimental Setup.** The fabricated nanodisk arrays were analyzed by a scanning electron microscope (JEOL JSM-7001 field emission scanning electron microscope). Optical absorption and reflection spectra of the fabricated arrays were obtained using a commercial UV−visible−near IR spectrophotometer (Hitachi U-4100).

**Electromagnetic Simulations.** Electromagnetic simulations were performed with the three-dimensional finite-difference time-domain (3D-FDTD) method.[31] The grid cell along all three dimensions is chosen as 2 nm. The dielectric permittivity of the sphere is set at 2.6. The dielectric constants for the Ag were obtained by fitting with the empirical dielectric constant of bulk Ag between 300 and 1900 nm following a Drude−Lorentzian model.[32] The plasma frequency and the loss of Ag are set to be $1.255 \times 10^{16}$ s$^{-1}$ and $0.68 \times 10^{14}$ s$^{-1}$, respectively.

*Conflict of Interest:* The authors declare no competing financial interest.

*Acknowledgment.* We acknowledge the financial support from National Science Council, Taiwan (grant numbers NSC 99-2112-M-006-015-MY2, NSC 99-2627-B-006-016-, NSC 100-2627-B-006-014-). We also acknowledge the collaboration of Center of Micro/Nano Science and Technology, National Cheng Kung University, Tainan, Taiwan. The National Center for High-Performance Computing of Taiwan and the Computer and Network of National Cheng Kung University are also acknowledged for use of their high-performance computing facilities. The equipment access and valuable suggestions from Professors Tzong-Fang Guo and Yung-Chiang Lan of the Department of Photonics, National Cheng Kung University, are also much appreciated.

## REFERENCES AND NOTES

1. Ritchie, R. H. Plasma Losses by Fast Electrons in Thin Films. *Phys. Rev.* **1957**, *1*, 874–881.
2. Halas, N. J.; Lal, S.; Link, S. Nano-Optics from Sensing to Waveguiding. *Nat. Photonics* **2007**, *1*, 641–648.
3. Van Duyne, R. P.; Bingham, J. M.; Anker, J. N.; Kreno, L. E. Gas Sensing with High-Resolution Localized Surface Plasmon Resonance Spectroscopy. *J. Am. Chem. Soc.* **2010**, *132*, 17358–17359.
4. Kall, M.; Chen, S. C.; Svedendahl, S.; Van Duyne, M.; Plasmon-Enhanced, R. P. Colorimetric ELISA with Single Molecule Sensitivity. *Nano Lett.* **2011**, *11*, 1826–1830.
5. Anker, J. N.; Hall, W. P.; Lyandres, O.; Shah, N. C.; Zhao, J.; Van Duyne, R. P. Biosensing with Plasmonic Nanosensors. *Nat. Mater.* **2008**, *7*, 442–453.
6. Hafner, J. H.; Mayer, K. M. Localized Surface Plasmon Resonance Sensors. *Chem. Rev.* **2011**, *111*, 3828–3857.
7. Haes, A. J.; Haynes, C. L.; McFarland, A. D.; Schatz, G. C.; Van Duyne, R. R.; Zou, S. L. Plasmonic Materials for Surface-Enhanced Sensing and Spectroscopy. *MRS Bull.* **2005**, *30*, 368–375.
8. Jeanmaire, D. L.; Vanduyne, R. P. Surface Raman Spectroelectrochemistry 0.1. Heterocyclic, Aromatic, and Aliphatic-Amines Adsorbed on Anodized Silver Electrode. *J. Electroanal. Chem.* **1977**, *84*, 1–20.
9. Talley, C. E.; Jackson, J. B.; Oubre, C.; Grady, N. K.; Hollars, C. W.; Lane, S. M.; Huser, T. R.; Nordlander, P.; Halas, N. J. Surface-Enhanced Raman Scattering from Individual Au Nanoparticles and Nanoparticle Dimer Substrates. *Nano Lett.* **2005**, *5*, 1569–1574.
10. Prodan, E.; Radloff, C.; Halas, N. J.; Nordlander, P. A Hybridization Model for the Plasmon Response of Complex Nanostructures. *Science* **2003**, *302*, 419–422.
11. Wang, H.; Brandl, D. W.; Nordlander, P.; Halas, N. J. Plasmonic Nanostructures: Artificial Molecules. *Acc. Chem. Res.* **2007**, *40*, 53–62.
12. Nordlander, P.; Halas, N. J.; Lal, S.; Chang, W. S.; Link, S. Plasmons in Strongly Coupled Metallic Nanostructures. *Chem. Rev.* **2011**, *111*, 3913–3961.
13. Odom, T. W.; Zhou, W. Tunable Subradiant Lattice Plasmons by Out-of-Plane Dipolar Interactions. *Nat. Nanotechnol.* **2011**, *6*, 423–427.
14. Noginov, M. A.; Zhu, G.; Belgrave, A. M.; Bakker, R.; Shalaev, V. M.; Narimanov, E. E.; Stout, S.; Herz, E.; Suteewong, T.; Wiesner, U. Demonstration of a Spaser-Based Nanolaser. *Nature* **2009**, *460*, 1110–U68.
15. Zhang, X.; Oulton, R. F.; Sorger, V. J.; Zentgraf, T.; Ma, R. M.; Gladden, C.; Dai, L.; Bartal, G. Plasmon Lasers at Deep Subwavelength Scale. *Nature* **2009**, *461*, 629–632.

16. Yang, S. C.; Kobori, H.; He, C. L.; Lin, M. H.; Chen, H. Y.; Li, C. C.; Kanehara, M.; Teranishi, T.; Gwo, S. Plasmon Hybridization in Individual Gold Nanocrystal Dimers: Direct Observation of Bright and Dark Modes. *Nano Lett.* **2010**, *10*, 632–637.
17. Koh, A. L.; Fernandez-Dominguez, A. I.; McComb, D. W.; Maier, S. A.; Yang, J. K. W. High-Resolution Mapping of Electron-Beam-Excited Plasmon Modes in Lithographically Defined Gold Nanostructures. *Nano Lett.* **2011**, *11*, 1323–1330.
18. Chu, M. W.; Myroshnychenko, V.; Chen, C. H.; Deng, J. P.; Mou, C. Y.; de Abajo, F. J. G. Probing Bright and Dark Surface-Plasmon Modes in Individual and Coupled Noble Metal Nanoparticles Using an Electron Beam. *Nano Lett.* **2009**, *9*, 399–404.
19. Nelayah, J.; Kociak, M.; Stephan, O.; de Abajo, F. J. G.; Tence, M.; Henrard, L.; Taverna, D.; Pastoriza-Santos, I.; Liz-Marzan, L. M.; Colliex, C. Mapping Surface Plasmons on a Single Metallic Nanoparticle. *Nat. Phys.* **2007**, *3*, 348–353.
20. Nordlander, P.; Hao, F.; Larsson, E. M.; Ali, T. A.; Sutherland, D. S. Shedding Light on Dark Plasmons in Gold Nanorings. *Chem. Phys. Lett.* **2008**, *458*, 262–266.
21. Su, K. H.; Durant, S.; Steele, J. M.; Xiong, Y.; Sun, C.; Zhang, X. Raman Enhancement Factor of a Single Tunable Nanoplasmonic Resonator. *J. Phys. Chem. B* **2006**, *110*, 3964–3968.
22. Sun, C.; Su, K. H.; Valentine, J.; Rosa-Bauza, Y. T.; Ellman, J. A.; Elboudwarej, O.; Mukherjee, B.; Craik, C. S.; Shuman, M. A.; Chen, F. F.; Zhang, X. Time-Resolved Single-Step Protease Activity Quantification Using Nanoplasmonic Resonator Sensors. *ACS Nano* **2010**, *4*, 978–984.
23. Feth, N.; Enkrich, C.; Wegener, M.; Linden, S. Large-Area Magnetic Metamaterials via Compact Interference Lithography. *Opt. Express.* **2007**, *15*, 501–507.
24. Kuttge, M.; de Abajo, F. J. G.; Polman, A. Ultrasmall Mode Volume Plasmonic Nanodisk Resonators. *Nano Lett.* **2010**, *10*, 1537–1541.
25. Lee, S. W.; Lee, K. S.; Ahn, J.; Lee, J. J.; Kim, M. G.; Shin, Y. B. Highly Sensitive Biosensing Using Arrays of Plasmonic Au Nanodisks Realized by Nanoimprint Lithography. *ACS Nano* **2011**, *5*, 897–904.
26. Hulteen, J. C.; Vanduyne, R. P. Nanosphere Lithography - A Materials General Fabrication Process for Periodic Particle Array Surfaces. *J. Vac. Sci. Technol., A* **1995**, *13*, 1553–1558.
27. Hou, C. H.; Tseng, S. Z.; Chan, C. H.; Chen, T. J.; Chien, H. T.; Hsiao, F. L.; Chiu, H. K.; Lee, C. C.; Tsai, Y. L.; Chen, C. C. Output Power Enhancement of Light-Emitting Diodes via Two-Dimensional Hole Arrays Generated by a Monolayer of Microspheres. *Appl. Phys. Lett.* **2009**, *95*, 133105.
28. Wu, W.; Katsnelson, A.; Memis, O. G.; Mohseni, H.; Deep Sub-Wavelength, A Process for the Formation of Highly Uniform Arrays of Nanoholes and Nanopillars. *Nanotechnology* **2007**, *18*, 485302.
29. Chang, C. H.; Tian, L.; Hesse, W. R.; Gao, H.; Choi, H. J.; Kim, J. G.; Siddiqui, M.; Barbastathis, G. From Two-Dimensional Colloidal Self-Assembly to Three-Dimensional Nanolithography. *Nano Lett.* **2011**, *11*, 2533–2537.
30. Ormonde, A. D.; Hicks, E. C. M.; Castillo, J.; Van Duyne, R. P. Nanosphere Lithography: Fabrication of Large-Area Ag Nanoparticle Arrays by Convective Self-Assembly and Their Characterization by Scanning UV-Visible Extinction Spectroscopy. *Langmuir* **2004**, *20*, 6927–6931.
31. Taflove, A.; Hagness, S. C. *Computational Electrodynamics: the Finite-Di□erence Time-Domain Method*, 3rd ed.; Artech House: Boston, 2005; p xxii.
32. Lee, T. W.; Gray, S. K. Subwavelength Light Bending by Metal Slit Structures. *Opt. Express.* **2005**, *13*, 9652–9659.